Unimodal polyethylenes of high linearity and narrow dispersity by using *ortho*-4,4'-dichlorobenzhydryl-modified bis(imino)pyridyl-iron catalysts†

Tian Liu,[ab] Yanping Ma, [ID][a] Gregory A. Solan,*[ac] Yang Sun[a] and Wen-Hua Sun [ID] *[abd]

Six different examples of 4,4'-dichlorobenzhydryl-substituted 2,6-bis(arylimino)pyridyl-iron(II) chloride complex, [2-{{2,6-((*p*-ClPh)$_2$CH)$_2$-4-MeC$_6$H$_2$}N=CMe)-6-(ArN=CMe)C$_5$H$_3$N]FeCl$_2$ (Ar = 2,6-Me$_2$C$_6$H$_3$ **Fe1**, 2,6-Et$_2$C$_6$H$_3$ **Fe2**, 2,6-^{i}Pr$_2$C$_6$H$_3$ **Fe3**, 2,4,6-Me$_3$C$_6$H$_2$ **Fe4**, 2,6-Et$_2$-4-MeC$_6$H$_2$ **Fe5**, 2,6-((*p*-ClPh)$_2$CH)$_2$-4-MeC$_6$H$_2$ **Fe6**), have been synthesized in good yield and characterized by various spectroscopic and analytical techniques. The molecular structures of **Fe2** and **Fe5** emphasize the uneven steric protection of the ferrous center imposed by the unsymmetrical *N,N,N'*-chelate. When treated with either MAO or MMAO (modified-MAO) as activators, **Fe1–Fe5** exhibited very high productivities at elevated temperature with peak performance of 21.59 × 10^6 g PE mol^{-1}(Fe) h^{-1} for **Fe5**/MMAO at 50 °C and 15.65 × 10^6 g PE mol^{-1}(Fe) h^{-1} for **Fe1**/MAO at 60 °C. By contrast, the most sterically hindered **Fe6** was either inactive (using MAO) or displayed very low activity (using MMAO). As a further feature, this class of iron catalyst was capable of displaying long lifetimes with catalytic activities up to 10.77 × 10^6 g PE mol^{-1}(Fe) h^{-1} observed after 1 h. In all cases, strictly linear and unimodal polyethylene was formed with narrow dispersity, while the polymer molecular weight was strongly influenced by the aluminoxane co-catalyst (M_w using MAO > MMAO) and also by the steric properties of the second *N*-aryl group (up to 32.9 kg mol^{-1} for **Fe3**/MAO).

Introduction

Over recent years, rapid developments have been seen in the design of iron (and cobalt) complexes as catalysts for olefin polymerization. These have been largely inspired by the pioneering disclosures in the late 1990s that bis(imino)pyridine-chelated examples can display high catalytic activity (**A**, Chart 1).[1–11] In a manner similar to the industrialization of Ziegler–Natta catalysts, researchers have been committed to improving both the activity and thermal stability of iron catalysts as well as the performance characteristics of the resulting polyolefinic materials.[12–24] From an industrial standpoint, iron is one of the most abundant elements on the earth which offers, on account of its cost effectiveness, considerable
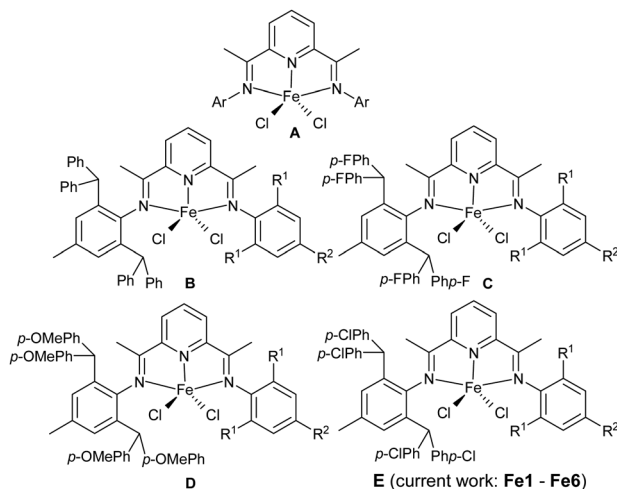
[a] *Key Laboratory of Engineering Plastics and Beijing National Laboratory for Molecular Sciences, Institute of Chemistry, Chinese Academy of Sciences, Beijing 100190, China. E-mail: whsun@iccas.ac.cn; Fax: +86-10-62618239; Tel: +86-10-62557955*

[b] *CAS Research/Education Center for Excellence in Molecular Sciences, University of Chinese Academy of Sciences, Beijing 100049, China*

[c] *Department of Chemistry, University of Leicester, University Road, Leicester LE1 7RH, UK. E-mail: gas8@leicester.ac.uk; Tel: +44-116-2522096*

[d] *State Key Laboratory for Oxo Synthesis and Selective Oxidation, Lanzhou Institute of Chemical Physics Chinese Academy of Sciences, Lanzhou 730000, China*

Chart 1 Parent bis(imino)pyridyl-iron precatalyst **A** and its *ortho*-CH(*p*-RC$_6$H$_4$)$_2$-substituted derivatives, **B** (R = H), **C** (R = F), **D** (R = OMe), and the target of the current work **E** (R = Cl).

opportunities to be integrated into a commercial process. However, the sensitivity of **A**-derived catalysts towards deactivation at higher operating temperatures has somewhat hindered their further industrial development.[26] In particular, pathways involving alkylation reactions or deprotonation chemistry involving the imino-C methyl groups in the *N,N,N*-ligand frame have been proposed as likely deactivation routes.[25] As a consequence, research endeavors in this area have largely focused on the improvement of the thermal stability of bis(imino)pyridyl-iron catalysts while maintaining or enhancing the overall effectiveness of the polymerization process.[27–37]

In the main, two strategies have been employed with a view to improve thermal stability and activity of *N,N,N*-iron catalysts, namely modification of the substituents on the *N*-aryl groups in **A** or changes to the ligand framework itself.[38–51] Among these, most effort has been dedicated to the introduction of large sterically hindered substituents to the *N*-aryl group in **A** that not only retain the high catalytic activity, but also improve the thermal stability of the catalyst.[49,50] Based on research conducted by our group and others, we have found that the introduction of *ortho*-benzhydryl (CHPh$_2$) substituents to a single *N*-aryl group in an unsymmetrical version of **A** (**B**, Chart 1) can be beneficial to the thermal stability of the iron catalyst.[52] Furthermore, when the benzhydryl group in **B** was affixed with electron-withdrawing *para*-fluoride substituents (**C**, Chart 1), improved catalytic activity was observed whereas the molecular weight of the polymer reduced.[53] Conversely, the introduction of an electron-donating *para*-methoxy group to the benzhydryl substituent (**D**, Chart 1) significantly increased the molecular weight of the polyethylene whereas the catalytic activity lowered.[54] Evidently, the electronic properties of the substituents on the benzhydryl groups have a crucial influence on the catalytic performance of the bis(imino)pyridine-iron complexes and the properties of the resulting polyethylene.

To further explore the influence of electronic effects on the performance of benzhydryl-substituted bis(imino)pyridine-iron catalysts, we target in this work a series of iron precatalysts incorporating *N*-2,6-bis(4,4′-dichlorobenzhydryl)-4-methylphenyl groups (**E**, Chart 1). More specifically, we disclose six examples of **E** (**Fe1–Fe6**) in which the second *N*-aryl group is systematically modified in terms of its steric and electronic properties. All iron precatalysts are subject to a comprehensive polymerization evaluation that explores how run temperature, co-catalyst, run time and ethylene pressure can impact on performance and polymer properties. In addition, full characterization for the new complexes is described.

Results and discussion

Synthesis and characterization

The ferrous chloride complexes, [2-{{2,6-((*p*-ClPh)$_2$CH)$_2$-4-MeC$_6$H$_2$}N=CMe}-6-(ArN=CMe)C$_5$H$_3$N]FeCl$_2$ (Ar = 2,6-Me$_2$C$_6$H$_3$ **Fe1**, 2,6-Et$_2$C$_6$H$_3$ **Fe2**, 2,6-^{i}Pr$_2$C$_6$H$_3$ **Fe3**, 2,4,6-Me$_3$C$_6$H$_2$ **Fe4**, 2,6-Et$_2$-4-MeC$_6$H$_2$ **Fe5**) and [2,6-{{2,6-((*p*-ClPh)$_2$CH)$_2$-4-MeC$_6$H$_2$}N=CMe}$_2$C$_5$H$_3$N]FeCl$_2$ (**Fe6**), were prepared in good yield by interaction of the corresponding bis(imino)pyridine, **L1–L6**, with iron(II) chloride
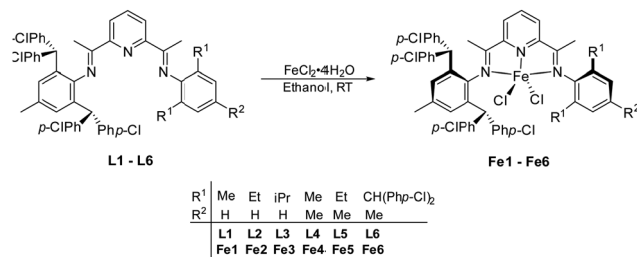
Scheme 1   Synthesis of *N,N,N*-iron(II) chloride complexes **Fe1–Fe6**.

hexahydrate in ethanol at ambient temperature (Scheme 1). The compounds, **L1–L6**, were prepared in two-steps from 2,6-diacetylpyridine using a previously described procedure.[22] All iron complexes were characterized by FT-IR spectroscopy, ESI mass spectrometry and elemental analysis. In addition, the molecular structures of **Fe2** and **Fe5** were determined using single-crystal X-ray diffraction.

Crystals of **Fe2** and **Fe5** suitable for the X-ray determinations were grown as described in the Experimental section (see later). Views of **Fe2** and **Fe5** are depicted in Fig. 1 and 2, respectively, while selected bond lengths and angles are listed in Table 1.

The coordination geometry of both complexes can be described as distorted square pyramidal with N1, N2, N3 and Cl2 defining the square base and Cl1 the apical position (N(2)–Fe(1)–Cl(1): 89.61° (**Fe2**), 93.11° (**Fe5**)).[51,52] More specifically the degree of distortion can be quantified in terms of the tau value (with tau = 0 perfectly square pyramidal and tau = 1 perfectly trigonal bipyramid),[64] with **Fe2** being 0.23 and **Fe5** 0.17. The iron atom itself sits at a distance of 0.531 Å above the basal plane for **Fe2** and 0.571 Å for **Fe5**. For both structures, the planes of the inequivalent *N*-aryl groups are inclined almost perpendicularly to the neighboring imine vectors with dihedral angles of 84.02° and 87.98° for **Fe2**, and 77.50° and 87.15° for
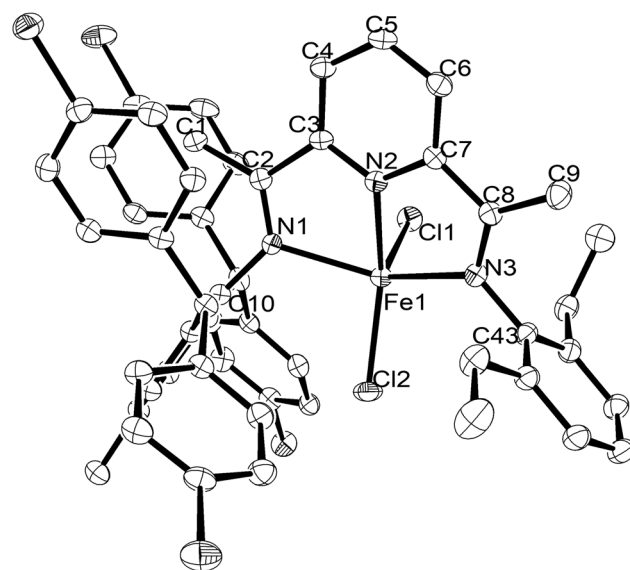
Fig. 1   ORTEP representation of **Fe2** with the thermal ellipsoids at the 30% probability level. All hydrogen atoms have been omitted for clarity.
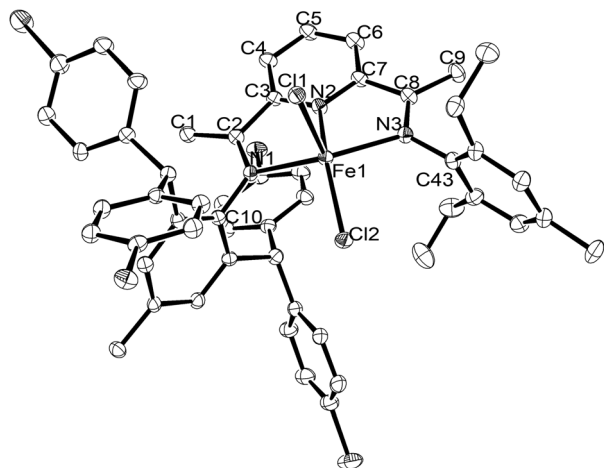
Fig. 2 ORTEP representation of **Fe5** with the thermal ellipsoids at the 30% probability level. All hydrogen atoms have been omitted for clarity.

Table 1 Selected bond lengths and angles for **Fe2** and **Fe5**

	Fe2	**Fe5**
	Bond lengths (Å)	
Fe(1)–N(1)	2.206(4)	2.234(4)
Fe(1)–N(2)	2.068(4)	2.062(4)
Fe(1)–N(3)	2.207(4)	2.200(4)
Fe(1)–Cl(1)	2.3375(13)	2.3199(13)
Fe(1)–Cl(2)	2.2384(14)	2.2513(12)
	Bond Angles (deg)	
N(1)–Fe(1)–N(2)	72.85(14)	73.19(14)
N(1)–Fe(1)–N(3)	139.59(14)	139.62(14)
N(2)–Fe(1)–N(3)	73.99(15)	73.87(15)
N(1)–Fe(1)–Cl(2)	100.12(11)	99.45(10)
N(2)–Fe(1)–Cl(2)	153.34(11)	150.22(12)
N(3)–Fe(1)–Cl(2)	99.18(11)	97.61(11)
N(1)–Fe(1)–Cl(1)	95.11(10)	99.07(10)
N(2)–Fe(1)–Cl(1)	89.61(10)	93.11(12)
N(3)–Fe(1)–Cl(1)	107.13(11)	105.41(11)
Cl(2)–Fe(1)–Cl(1)	116.87(6)	116.66(5)

Fe5. In terms of the Fe–N bond lengths, it is apparent that there are some differences with the central Fe–$N_{pyridine}$ bond length [2.068(4) (**Fe2**), 2.062(4) (**Fe5**) Å] markedly shorter than the exterior Fe–N_{imine} ones [2.200(4)–2.234(4) Å]. This observation is widespread in this class of complex and highlights more effective coordination of the pyridine nitrogen with the iron center.[57] Scrutiny of the Fe–N_{imine} distances reveals little variation in **Fe2**, whereas in **Fe5**, some minor difference is apparent with that involving the bulkier 2,6-bis(4,4′-dichlorobenzhydryl)-4-methyl-phenyl-substituted N_{imine} slightly longer [Fe(1)–N(1) 2.234(4) Å] than its 2,6-diethyl-4-methylphenyl-N_{imine} comparator [Fe(1)–N(3) 2.200(4) Å], suggesting steric factors exert some influence. With regard to the planarity of the bis(imino)pyridine, some minimal deviation between the neighboring imine vectors and the pyridine ring is also evident as is evidenced by the torsion angles for N(1)–C(2)–C(3)–N(2) [−3.38° (**Fe2**), 1.71° (**Fe5**)] and N(3)–C(8)–C(7)–N(2) [5.07° (**Fe2**), −2.86° (**Fe5**)]. There are no intermolecular contacts of note.

In the mass spectra of **Fe1**–**Fe6**, fragmentation peaks corresponding to the loss of one chloride are seen in each case, while their FT-IR spectra reveal stretching vibrations for the $\nu(C{=}N)_{imine}$ groups in the range of 1607–1614 cm^{-1}. When compared to their free ligands, **L1**–**L6**, these stretching vibrations are generally lower in wavenumber by *ca.* 30 cm^{-1}, which provides further evidence of successful coordination of both N_{imine} donors of the ligand to the metal center.[58]

Ethylene polymerization studies

To permit **Fe1**–**Fe6** to be evaluated as precatalysts for ethylene polymerization, methylaluminoxane (MAO) and modified methylaluminoxane (MMAO) were deployed as co-catalysts. For each co-catalyst, **Fe1** was utilized as the test precatalyst to allow an optimal set of polymerization conditions to be identified in terms of run temperature, molar ratio of Al : Fe, run time and ethylene pressure. Typically, the runs were performed in toluene with ethylene pressure initially set at 10 atm. The resulting polyethylenes were then analyzed by gel permeation chromatography (GPC) and differential scanning calorimetry (DSC) to shed light on the polymer properties and in turn catalyst behavior.

Ethylene polymerization using Fe1–Fe6 with MAO as co-catalyst. Firstly, **Fe1**/MAO was investigated as the catalyst system with the run temperature varied from 40 °C to 80 °C with the Al : Fe ratio kept at 2000 : 1 and the run time at 30 min (entries 1–5, Table 2). Inspection of the data reveals the catalytic activity to initially increase with temperature reaching a peak value of 10.46 × 10^6 g PE mol^{-1}(Fe) h^{-1} at 60 °C (entry 3, Table 2), and then decrease to 8.62 × 10^6 g PE mol^{-1}(Fe) h^{-1} at 80 °C; this loss in performance at temperatures in excess of 60 °C can be attributed to the onset of catalyst deactivation and the lower solubility of ethylene in the solvent at these

Table 2 Ethylene polymerization results using **Fe1**–**Fe6** and MAO at $P_{C_2H_4}$ = 10 atm^a

Entry	Precat.	T (°C)	Al : Fe	t (min)	Activity^b	$M_w{}^c$	$M_w/M_n{}^c$	$T_m{}^d$ (°C)
1	**Fe1**	40	2000	30	2.43	77.0	3.9	130.7
2	**Fe1**	50	2000	30	3.37	67.3	3.5	129.2
3	**Fe1**	60	2000	30	10.46	50.0	2.0	132.7
4	**Fe1**	70	2000	30	10.01	23.3	2.8	130.7
5	**Fe1**	80	2000	30	8.62	16.1	2.8	130.5
6	**Fe1**	60	1500	30	8.44	71.9	3.9	131.0
7	**Fe1**	60	2500	30	15.65	26.7	4.1	129.2
8	**Fe1**	60	3000	30	13.87	15.7	3.0	132.3
9	**Fe1**	60	3500	30	13.32	10.0	2.8	129.6
10	**Fe1**	60	2500	5	39.24	5.4	1.6	128.0
11	**Fe1**	60	2500	15	25.06	12.5	3.1	134.8
12	**Fe1**	60	2500	45	11.97	41.1	6.2	135.1
13	**Fe1**	60	2500	60	9.43	53.7	6.4	131.4
14^e	**Fe1**	60	2500	30	13.87	20.8	5.9	131.8
15^f	**Fe1**	60	2500	30	0.38	0.9	1.3	123.5
16	**Fe2**	60	2500	30	11.64	21.0	3.8	131.1
17	**Fe3**	60	2500	30	6.48	32.9	2.8	135.1
18	**Fe4**	60	2500	30	14.82	10.5	1.8	130.8
19	**Fe5**	60	2500	30	11.92	16.4	2.8	130.1
20	**Fe6**	60	2500	30	—	—	—	—

^{a} Conditions: 2.0 μmol of iron precatalyst, 10 atm ethylene, 100 mL toluene. ^{b} Activity: 10^6 g PE per mol (Fe) per h. ^{c} M_w in kg per mol. M_w and M_w/M_n measured by GPC. ^{d} Measured by DSC. ^{e} 5 atm. ^{f} 1 atm.
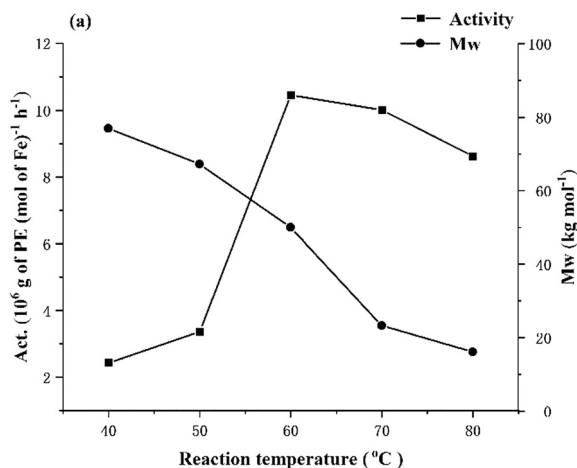
Fig. 3 For **Fe1**/MAO: plots of catalytic activity and molecular weight of the polymer *versus* reaction temperature (entries 1–5, Table 2).

temperatures.[59] Nonetheless, the observed polymerization activity at 80 °C is greater than those of a host of cobalt or iron analogues,[51,54] which would point towards appreciable thermal stability. In terms of the molecular weight of the polyethylene, this was observed to decrease at higher run temperature, in accordance with an increased rate of chain termination (Fig. 3).

Next, the molar ratio of Al:Fe using **Fe1**/MAO was varied between 1500:1 and 3500:1 with the run temperature fixed at 60 °C (entries 3, 6–9, Table 2). With the ratio at 2500:1, the highest activity of 15.65×10^6 g PE mol^{-1}(Fe) h^{-1} was achieved (entry 7, Table 2). On the other hand, the highest molecular weight polymer ($M_w = 71.9$ kg mol^{-1}) was obtained with the Al:Fe ratio at 1500:1, while further increasing the Al:Fe ratio to 3500:1, the polymer molecular weight decreased to 10.0 kg mol^{-1} (Fig. 4). This drop in molecular weight would signify that higher ratios foster quicker chain transfer from the iron active center to the aluminum species and concomitant chain termination.[60] As a further notable feature was the relatively narrow dispersity (M_w/M_n range: 2.0–4.0) displayed
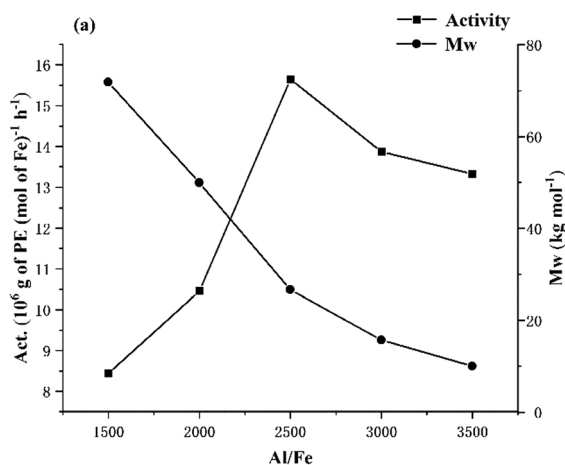
by these polyethylenes that highlights the good control and single-site-like nature of the active species (Fig. S2, ESI†). With regard to the polyethylene, these were of high linearity (T_m range: 129.2–132.7 °C) as is common using iron ethylene polymerization catalysts.[54]

With a view to exploring the lifetime of the active species formed using **Fe1**/MAO, the polymerization runs were performed at set run times between 5 and 60 min with the temperature kept at 60 °C and the Al:Fe ratio fixed at 2500:1 (entries 7, 10–14, Table 2). The maximum activity of 39.24×10^6 g PE mol^{-1}(Fe) h^{-1} was observed after 5 min, indicating that the active species was rapidly generated following addition of MAO and then progressively deactivated as the catalytic run time elapsed (Fig. 5). Although uncertain, it is plausible that an irreversible structural change of the catalyst occurs at high temperature leading to the observed deactivation of the catalyst. Alternatively, poisoning of the catalyst by trace impurities in the reaction system could account for this loss in activity. With respect to the ethylene pressure, a drop-in catalytic activity was noted as the pressure was lowered (entries 7, 14 and 15, Table 2), with a value of 15.65×10^6 g PE mol^{-1}(Fe) h^{-1} obtained at $P_{C_2H_4} = 10$ atm that reduced to 13.87×10^6 g PE mol^{-1}(Fe) h^{-1} at 5 atm and then more dramatically decreased to 0.38×10^6 g PE mol^{-1}(Fe) h^{-1} at 1 atm. This dependency of the polymerization activity on the pressure can be attributed to the relative rates of insertion and ethylene coordination which can be enhanced at higher ethylene pressures.[61]

With the optimum polymerization conditions identified for **Fe1**/MAO (*viz.* 60 °C, Al:Fe ratio of 2500:1, 10 atm ethylene and 30 min), the remaining iron complexes (**Fe2–Fe6**) were investigated as precatalysts for ethylene polymerization (entries 16–20, Table 2). In general, all iron/MAO systems displayed very good catalytic performance (range in activity: 6.48–15.65×10^6 g PE mol^{-1}(Fe) h^{-1}), with the exception of **Fe6** which proved inactive. This latter observation can be attributed to the excessive steric hindrance provided by the four bulky 4,4′-dichlorobenzhydryl *ortho*-substituents in **Fe6** which impedes ethylene

Fig. 4 For **Fe1**/MAO: plots of catalytic activity and molecular weight of the polymer *versus* Al:Fe molar ratio (entries 3 and 6–9, Table 2).
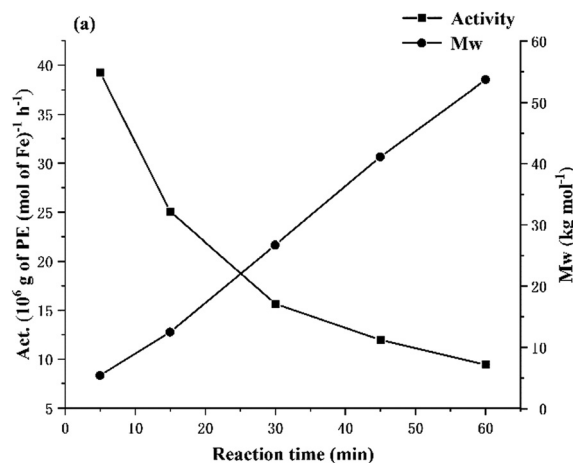

Fig. 5 For **Fe1**/MAO: plots of catalytic activity and molecular weight of the polymer *versus* reaction time (entries 7 and 10–13, Table 2).
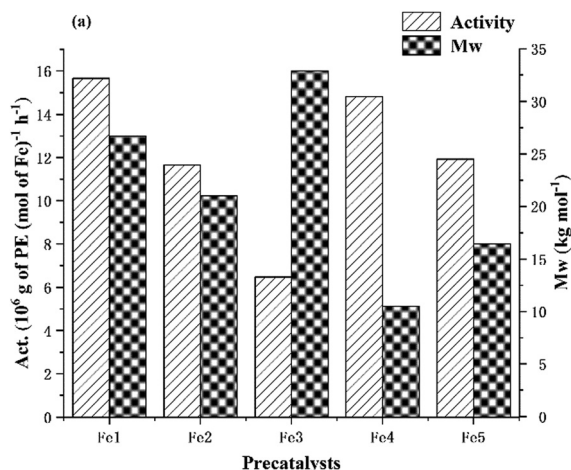
Fig. 6 For **Fe1–Fe5** using MAO as co-catalyst: a bar chart showing catalytic activity and molecular weight of the polymer *versus* the type of iron precatalyst (entries 7 and 16–20, Table 2).

Table 3 Ethylene polymerization results using **Fe1–Fe6** and MMAO at $P_{C_2H_4}$ = 10 atm[a]

Entry	Precat.	T (°C)	Al : Fe	t (min)	Activity[b]	M_w[c]	M_w/M_n[c]	T_m[d] (°C)
1	**Fe1**	40	2500	30	8.70	18.7	3.5	126.4
2	**Fe1**	50	2500	30	17.31	15.4	2.9	128.3
3	**Fe1**	60	2500	30	15.11	7.6	1.9	128.6
4	**Fe1**	70	2500	30	13.44	4.7	1.6	125.6
5	**Fe1**	80	2500	30	5.84	2.6	1.6	122.6
6	**Fe1**	50	2000	30	13.80	16.0	1.4	127.4
7	**Fe1**	50	3000	30	17.61	6.5	2.0	128.8
8	**Fe1**	50	3500	30	18.12	4.7	1.3	131.2
9	**Fe1**	50	4000	30	15.69	4.0	1.7	124.7
10	**Fe1**	50	3500	5	57.12	3.0	1.5	123.9
11	**Fe1**	50	3500	15	28.02	4.6	1.8	125.8
12	**Fe1**	50	3500	45	13.09	7.1	2.7	127.2
13	**Fe1**	50	3500	60	10.77	9.1	3.4	128.3
14[e]	**Fe1**	50	3500	30	13.80	3.5	2.3	127.1
15[f]	**Fe1**	50	3500	30	0.12	0.9	1.6	122.6
16	**Fe2**	50	3500	30	20.12	12.7	4.2	129.8
17	**Fe3**	50	3500	30	5.51	13.7	2.0	124.5
18	**Fe4**	50	3500	30	16.66	4.4	1.5	125.7
19	**Fe5**	50	3500	30	21.59	3.4	1.4	128.9
20	**Fe6**	50	3500	30	0.29	4.6	2.1	127.3

[a] Conditions: 2.0 μmol of iron precatalyst, 10 atm ethylene, 100 mL toluene. [b] Activity: 10^6 PE per mol (Fe) per h. [c] M_w in kg per mol. M_w and M_w/M_n measured by GPC. [d] Measured by DSC. [e] 5 atm. [f] 1 atm.

coordination. With regard to the relative activities of **Fe1–Fe5**, their levels decreased in the order: **Fe1** (2,6-dimethyl) > **Fe4** (2,4,6-trimethyl) > **Fe5** (2,6-diethyl-4-methyl) > **Fe2** (2,6-diethyl) > **Fe3** (2,6-diisopropyl) (Fig. 6). This trend emphasizes the role played by the steric properties of these *ortho*-substituents on the amenability to ethylene monomer coordination and insertion.[62] In particular, it is apparent that the increase in steric properties from 2,6-diethyl to 2,6-diisopropyl leads to a steady decline in activity. By contrast, the variation in molecular weight with respect to iron precatalyst follows the order, **Fe3** > **Fe1** > **Fe2** > **Fe5** > **Fe4**, which indicates that greater hindrance leads to higher molecular weight polymer (up to 32.9 kg mol^{-1} for **Fe3**). As can be seen in Fig. S4 (ESI†), the resulting polyethylenes additionally showed reasonably narrow dispersity for all **Fe**/MAO combinations (M_w/M_n range: 1.8–3.8) in line with the good control displayed by the catalyst.

Ethylene polymerization using Fe1–Fe6 with MMAO as co-catalyst. As the nature of the co-catalyst can have an important influence on catalytic performance, MMAO was also investigated, and a similar optimization process was conducted with **Fe1** again used as the benchmark precatalyst (Table 3).

With the Al : Fe ratio fixed at 2500 : 1, the polymerization runs using **Fe1**/MMAO were performed at temperatures between 40 and 80 °C (entries 1–5, Table 3). The highest activity of 17.31 × 10^6 g PE mol^{-1}(Fe) h^{-1} was achieved at 50 °C, while further increasing the temperature to 80 °C saw the activity decrease to 5.84 × 10^6 g PE mol^{-1}(Fe) h^{-1} in line with deactivation of the catalyst occurring (Fig. 7). Similarly, the molecular weight of the polymer dropped from 18.7 to 2.6 kg mol^{-1} as a result of more effective chain termination occurring with increased temperature. By comparison with **Fe1**/MAO over a comparable temperature range, the polyethylene displayed much lower molecular weight and in turn the melting temperatures of the polymers were lower (T_m range: 122.6–128.6 °C).

The influence of Al : Fe molar ratio on the performance of **Fe1**/MMAO was then explored with the ratio varied between 2000 : 1 and 4000 : 1 and the run temperature maintained at
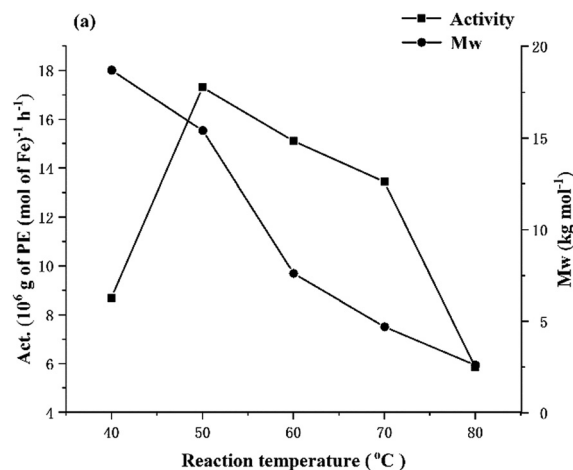

Fig. 7 For **Fe1**/MMAO: plots of catalytic activity and molecular weight of the polymer *versus* reaction temperature.

50 °C (entries 2, 6–9, Table 3). With the ratio at 3500 : 1, the uppermost activity of 18.12 × 10^6 g PE mol^{-1}(Fe) h^{-1} was obtained which then dropped to 15.69 × 10^6 g PE mol^{-1}(Fe) h^{-1} at 4000 : 1 as chain transfer to aluminum became more prominent.[63] Unimodal and narrowly disperse polyethylene (M_w/M_n range: 1.3–2.9) was obtained in agreement with the existence of single-site active species at a run temperature of 50 °C.

The time/activity profile of **Fe1**/MMAO was then investigated with the polymerization runs performed between 5 and 60 min (entries 8, 10–13, Table 3). As with **Fe1**/MAO, a short period of 5 min was sufficient to produce the active species leading to the highest activity of 57.12 × 10^6 g PE mol^{-1}(Fe) h^{-1}. As the run

time was extended beyond 5 min, the active species gradually deactivated resulting in lower activities with the level reaching 10.77×10^6 g PE mol^{-1}(Fe) h^{-1} after 1 h. Furthermore, and mirroring the MAO study, reducing the ethylene pressure greatly lowered the catalytic activity from 18.12×10^6 g PE mol^{-1}(Fe) h^{-1} at $P_{C_2H_4}$ = 10 atm to 0.12×10^6 g PE mol^{-1}(Fe) h^{-1} at 1 atm.

On the basis of the optimized parameters established for **Fe1**/MMAO namely, run temperature = 50 °C, Al : Fe molar ratio = 3500 : 1, $P_{C_2H_4}$ = 10 atm and run time = 30 min, the remaining iron precatalysts **Fe2–Fe6** were screened and their catalytic performance compared with **Fe1**/MAO. With the exception of **Fe6**, all the iron complexes exhibited high activities (range: $5.51–21.59 \times 10^6$ g PE mol^{-1}(Fe) h^{-1}), with levels in general exceeding that seen using MAO as co-catalyst (range: $6.48–15.65 \times 10^6$ g PE mol^{-1}(Fe) h^{-1}). In terms of the relative performance, these fell in the order: **Fe5** (2,6-diethyl-4-methyl) > **Fe2** (2,6-diethyl) > **Fe1** (2,6-dimethyl) > **Fe4** (2,4,6-trimethyl) > **Fe3** (2,6-diisopropyl) ≫ **Fe6** (2,6-bis(4,4′-dichlorobenzhydryl)-4-methyl) (Fig. 8). Once again, the activity exhibited by **Fe6** was found at the bottom end of the range suggesting that the excessive steric hindrance around the active center, inhibits the coordination and insertion of ethylene monomer.[62] On the other hand, the range in molecular weights of the polyethylenes produced was less than with MAO [3.4–13.7 kg mol^{-1} *vs.* 10.5–32.9 kg mol^{-1} (MAO)], which was reflected by the lower melting temperature range [124.5–129.8 °C *vs.* 129.2–135.1 °C (MAO)]. Nonetheless, all polyethylenes possessed narrow dispersity and unimodal distributions.

As is evident from the values of the melting temperatures of the polyethylenes shown in Tables 2 and 3, these materials all display a linear backbone. To lend further support for this linearity and to cast some light on their end-group composition, samples produced using **Fe1**/MAO at 60 °C (M_w = 26.7 kg mol^{-1}; entry 7, Table 2) and **Fe1**/MMAO at 50 °C (M_w = 4.7 kg mol^{-1}; entry 8, Table 3) were selected and characterized by ^{13}C NMR spectroscopy. To engender suitable solubility, the spectra were recorded at 100 °C in 1,1,2,2-tetrachloroethane-d$_2$. As is characteristic for both samples, the spectra show high intensity singlets at around δ 30.00 ppm (see Fig. 9 and Fig. S9, ESI†)
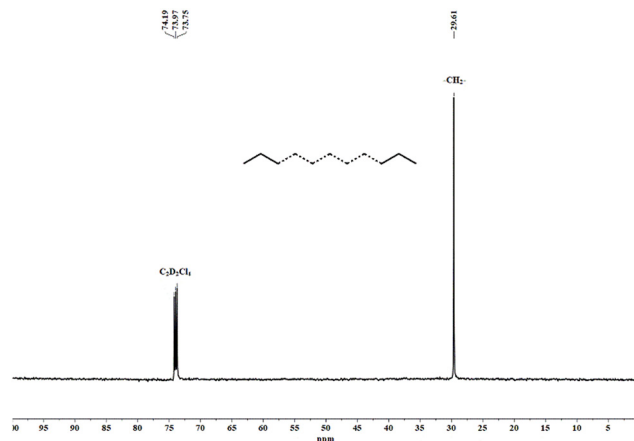

Fig. 9 ^{13}C NMR spectrum of the polyethylene obtained using **Fe1**/MAO at 60 °C (entry 7, Table 2); recorded in 1,1,2,2-tetrachloroethane-d$_2$ at 100 °C.

which can be assigned to the $-(CH_2)_n-$ repeat unit in support of the high linearity of the polyethylene. Furthermore, no peaks for saturated or unsaturated chain ends could be seen in the spectra which is likely due to high molecular weight of these samples.

Comparison of the current iron precatalysts with previously reported examples

With the intent to understand how the introduction of the *para*-chlorides to the benzhydryl phenyl groups in **E** affect the polymerization performance (*viz.* catalytic activity, polymer molecular weight and dispersity), a comparison with the previously reported unsymmetrical iron precatalysts, **B**, **C** and **D**,
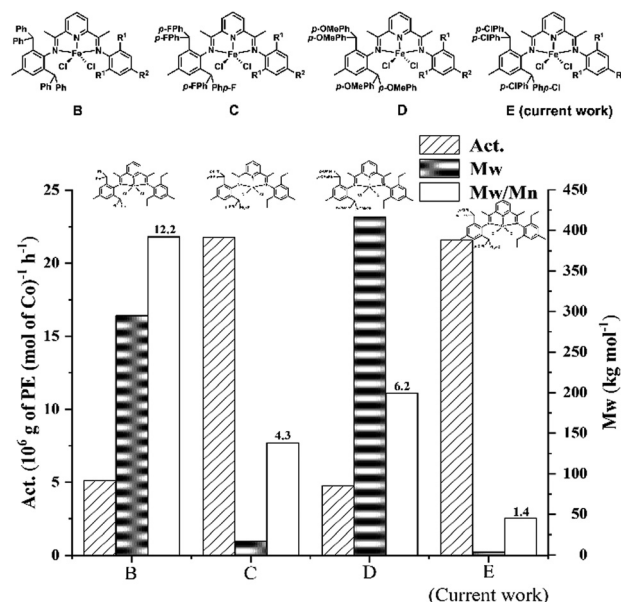

Fig. 10 Comparison of catalytic activity, polyethylene molecular weight and dispersity for **E** (this work) with that produced using **B**, **D** and **E**; all polymerization runs were performed at $P_{C_2H_4}$ = 10 atm using MMAO as co-catalyst under their optimal operating conditions (the reaction time of **B**, **D** and **E** is 30 min, **C** is 15 min).
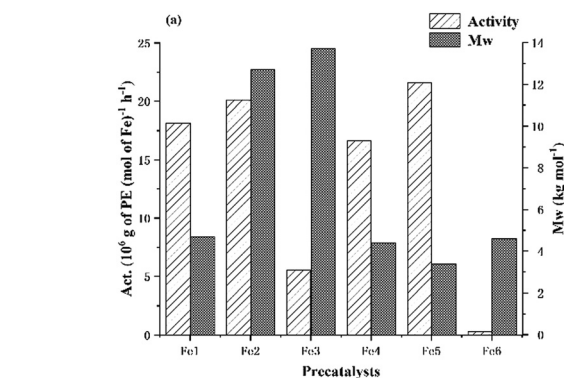

Fig. 8 For **Fe1–Fe6** with MMAO as co-catalyst: a bar chart showing catalytic activity and molecular weight of the polymer *versus* iron precatalyst (entries 8 and 16–20, Table 3).

was conducted (Fig. 10).[52–54] In particular, the most active system, **Fe5**/MMAO, was selected as a representative of the **E** class and performance data for the most structurally related examples of **B**, **C** and **D** compared; all polymerization runs were undertaken with MMAO under their optimized reaction conditions at 10 atm of C_2H_4.

In terms of the catalytic activity, it is evident that the 4,4'-dichlorobenzhydryl group in **E** has a positive impact on the level of activity with a value of 21.59×10^6 g PE mol^{-1}(Fe) h^{-1} seen over 30 min, which is higher than that for **B** (benzhydryl), **D** (4,4'-dimethoxybenzhydryl), and close to that seen for **C** (4,4'-difluorobenzhydryl) which was performed over 15 min. Moreover, the polyethylene generated using **E** exhibits the lowest molecular weight (M_w: 3.4 kg mol^{-1}) and narrowest dispersity (M_w/M_n: 1.4) and indeed has characteristics of a polyethylene wax. Overall, it is evident that **E** displays a closer similarity to it fluoride counterpart **C** than to **B** and **D**. The origin of these findings is uncertain but may relate to the electropositivity of the active iron center caused by the presence of the electron withdrawing *para*-halide. Nevertheless, it is clear that variations to the benzhydryl periphery, although remote from the metal center can not only enhance catalytic activity but also affect the molecular weight of the polymer.

Conclusions

To summarize, a series of unsymmetrical and symmetrical 2-[1-(2,6-bis(di(4-chlorophenyl)methyl)-4-methylphenylimino)ethyl]-6-[1-(arylimino)ethyl]pyridyl-iron(II) chloride complexes, **Fe1–Fe6**, were successfully synthesized by employing a straightforward and high yielding approach. Characterization of the complexes was achieved by using a range of techniques including single crystal X-ray diffraction for **Fe2** and **Fe5**. On activation with MAO and MMAO, **Fe1–Fe5** exhibited very good activities for ethylene polymerization with levels up to 21.59×10^6 g PE mol^{-1}(Fe) h^{-1} for **Fe5**/MMAO at 50 °C and 15.65×10^6 g PE mol^{-1}(Fe) h^{-1} for **Fe1**/MAO at 60 °C, producing strictly linear and narrowly disperse unimodal polyethylenes. Notably, the molecular weight of the polymer was influenced by not only the *N,N,N*'-ligand structure but also the aluminoxane employed with the MMAO runs displaying a predilection for forming lower molecular weight materials. In addition, by comparison with related benzhydryl-containing catalytic systems (**B–D**, Chart 1), we found that the introduction of the electron withdrawing Cl group is beneficial to the catalytic activity, while the catalysts with electron donating group (*e.g.* OCH_3) can generate higher molecular weight polyethylene. Overall, we feel these findings provide an important insight into the design of new catalysts based on electronic variations.

Experimental

General procedures

All manipulations making use of air- and moisture-sensitive compounds were carried out using standard Schlenk techniques or were performed in an inert atmosphere glovebox. Toluene, used for the polymerization studies, was dried over sodium and distilled under nitrogen prior to use. Methylaluminoxane (MAO, 1.30 M solution in toluene) and modified methylaluminoxane (MMAO, 1.93 M in *n*-heptane) were purchased from Anhiu Botai Electronic Materials Co. Other reagents were purchased from Aldrich, Acros or local suppliers (Beijing, China). High purity ethylene was purchased from Beijing Yansan Petrochemical Co. and used as received. The FT-IR spectra were recorded on a PerkinElmer System 2000 FT-IR spectrometer and elemental analysis were undertaken with a Flash EA 1112 microanalyzer. The molecular weights (M_w) and the dispersities (M_w/M_n) of the polyethylenes were carried out using an Agilent PL-GPC 220 GPC instrument (Beijing, China) at 150 °C with trichlorobenzene as the solvent. The melting points (T_m) of the polyethylenes were measured on a PerkinElmer TA-Q2000 differential scanning calorimeter (DSC) under a nitrogen atmosphere. In a typical procedure, a sample of about 5.0 mg was heated up to 160 °C at a rate of 20 °C min^{-1}, maintained for 5 min at 160 °C to remove the thermal history and then cooled to −20 °C at a rate of 20 °C min^{-1}. The ^{13}C NMR spectra of the polyethylenes were recorded on a Bruker AVANCE III 500 MHz instrument at 100 °C; a weighed amount of polyethylene (20–40 mg) was dissolved in 1,1,2,2-tetrachloroethane-d_2 (2 mL) with TMS as an internal standard. The bis(imino)pyridines, 2-{{2,6-((*p*-ClPh)$_2$CH)$_2$-4-MeC$_6$H$_2$}N=CMe}-6-(ArN=CMe)C$_5$H$_3$N (Ar = 2,6-Me$_2$C$_6$H$_3$ (**L1**), 2,6-Et$_2$C$_6$H$_3$ (**L2**), 2,6-^{i}Pr$_2$C$_6$H$_3$ (**L3**), 2,4,6-Me$_3$C$_6$H$_2$ (**L4**), 2,6-Et$_2$-4-MeC$_6$H$_2$ (**L5**)) and 2,6-{{2,6-((*p*-ClPh)$_2$CH)$_2$-4-MeC$_6$H$_2$}N=CMe}$_2$C$_5$H$_3$N (**L6**) were prepared using a previously reported route.[22]

Synthesis of Syntheses of [2-{{2,6-((*p*-ClPh)$_2$CH)$_2$-4-MeC$_6$H$_2$}N=CMe}-6-(ArN=CMe)C$_5$H$_3$N]FeCl$_2$ (Fe1–Fe6)

(a) Ar = 2,6-Me$_2$C$_6$H$_3$ (**Fe1**). Under a nitrogen atmosphere, FeCl$_2$·4H$_2$O (0.043 g, 0.22 mmol) and **L1** (0.20 g, 0.24 mmol) and were added together into a Schlenk tube and then freshly distilled ethanol (10 mL) introduced. The tube was sealed and the reaction mixture stirred for 12 h at room temperature to form a precipitate. Diethyl ether (10 mL) was added to complete the precipitation which was then filtered and washed with diethyl ether (3 × 10 mL). Following a period of drying under reduced pressure, **Fe1** was isolated as a blue powder (0.17 g, 82%). FT-IR (cm^{-1}): 2916 (w), 1614 ($\nu_{C=N}$, m), 1582 (m), 1489 (s), 1468 (m), 1405 (m), 1370 (m), 1317 (w), 1265 (m), 1211 (m), 1182 (w), 1090 (s), 1014 (s), 828 (s), 804 (s), 769 (m), 731 (m), 682 (m). HRMS (ESI) *m/z*: [M − Cl]$^+$, Calcd for C$_{50}$H$_{41}$Cl$_5$FeN$_3$ 914.1090, Found 914.1086. Anal. Calc. for C$_{50}$H$_{41}$Cl$_6$FeN$_3$ (952.44): C, 63.05; H, 4.34; N, 4.41%, Found: C, 63.03; H, 4.34; N, 4.12%.

(b) Ar = 2,6-Et$_2$C$_6$H$_3$ (**Fe2**). By adopting a similar procedure to that outlined for **Fe1** but with **L2** as the bis(imino)pyridine, **Fe2** was isolated as a blue powder (0.077 g, 75%). FT-IR (cm^{-1}): 2966 (w), 1973 (w), 1614 ($\nu_{C=N}$, m), 1582 (m), 1489 (s), 1454 (m), 1405 (m), 1371 (m), 1319 (w), 1267 (m), 1210 (m), 1180 (w), 1090 (s), 1014 (s), 870 (m), 831 (s), 804 (s), 767 (s), 732 (m), 683 (m). HRMS (ESI) *m/z*: [M − Cl]$^+$, Calcd for C$_{52}$H$_{45}$Cl$_5$FeN$_3$ 942.1403, Found 942.1402. Anal. Calc. for C$_{52}$H$_{45}$Cl$_6$FeN$_3$ (980.50): C, 63.70; H, 4.63; N, 4.29%, Found: C, 63.66; H, 4.58; N, 3.97%.

(c) Ar = 2,6-^{i}Pr$_2$C$_6$H$_3$ (**Fe3**). By adopting a similar procedure to that outlined for **Fe1** but with **L3** as the bis(imino)pyridine, **Fe3** was isolated as a blue powder (0.058 g, 56%). FT-IR (cm^{-1}): 2963 (w), 1973 (w), 1612 ($\nu_{C=N}$, m), 1581 (m), 1489 (s), 1462 (m), 1406 (m), 1372 (m), 1318 (w), 1268 (m), 1211 (m), 1182 (m), 1090 (s), 1054 (s), 1014 (s), 939 (w), 870 (m), 833 (s), 804 (s), 765 (m), 733 (m), 683 (m). HRMS (ESI) m/z: [M − Cl]$^+$, Calcd for C$_{54}$H$_{49}$Cl$_5$FeN$_3$ 970.1716, Found 970.1716. Anal. Calc. for C$_{54}$H$_{49}$Cl$_6$FeN$_3$ (1008.55): C, 64.31; H, 4.90; N, 4.17%, Found: C, 64.64; H, 4.97; N, 3.75%.

(d) Ar = 2,4,6-Me$_3$C$_6$H$_2$ (**Fe4**). By adopting a similar procedure to that outlined for **Fe1** but with **L4** as the bis(imino)pyridine, **Fe4** was isolated as a blue powder (0.091 g, 87%). FT-IR (cm^{-1}): 2912 (w), 1975 (w), 1607 ($\nu_{C=N}$, m), 1577 (m), 1489 (s), 1407 (m), 1373 (m), 1312 (w), 1271 (m), 1218 (m), 1184 (w), 1150 (w), 1090 (s), 1013 (s), 850 (m), 832 (s), 810 (s), 733 (m), 684 (m). HRMS (ESI) m/z: [M − Cl]$^+$, Calcd for C$_{51}$H$_{43}$Cl$_5$FeN$_3$ 928.1246, Found 928.1246. Anal. Calc. for C$_{51}$H$_{43}$Cl$_6$FeN$_3$ (966.47): C, 63.38; H, 4.48; N, 4.35%, Found: C, 63.20; H, 4.48; N, 4.12%.

(e) Ar = 2,6-Et$_2$-4-MeC$_6$H$_2$ (**Fe5**). By adopting a similar procedure to that outlined for **Fe1** but with **L5** as the bis(imino)pyridine, **Fe5** was isolated as a blue powder (0.076 g, 92%). FT-IR (cm^{-1}): 2967 (w), 1973 (w), 1612 ($\nu_{C=N}$, m), 1580 (m), 1489 (s), 1460 (m), 1406 (m), 1373 (m), 1321 (w), 1268 (m), 1214 (m), 1181 (m), 1090 (s), 1015 (s), 832 (s), 810 (s), 733 (m), 683 (m). HRMS (ESI) m/z: [M − Cl]$^+$, Calcd for C$_{53}$H$_{47}$Cl$_5$FeN$_3$ 956.1559, Found 956.1562. Anal. Calc. for C$_{53}$H$_{47}$Cl$_6$FeN$_3$ (994.53): C, 64.01; H, 4.76; N, 4.23%, Found: C, 64.03; H, 5.02; N, 3.89%.

(f) Ar = 2,6-((p-ClPh)$_2$CH)$_2$-4-MeC$_6$H$_2$ (**Fe6**). By adopting a similar procedure to that outlined for **Fe1** but with **L6** as the bis(imino)pyridine, **Fe6** was isolated as a blue powder (0.020 g, 25%). FT-IR (cm^{-1}): 1972 (w), 1607 ($\nu_{C=N}$, m), 1575 (m), 1489 (s), 1459 (m), 1405 (m), 1371 (m), 1269 (m), 1214 (m), 1091 (s), 1015 (s), 831 (s), 801 (s), 731 (m), 684 (m). Anal. Calc. for C$_{75}$H$_{55}$Cl$_{10}$FeN$_3$ (1408.63): C, 63.95; H, 3.94; N, 2.98%, Found: C, 63.81; H, 3.95; N, 2.82%.

X-ray crystallographic studies

Single crystals of **Fe2** and **Fe5** suitable for the X-ray determinations were obtained by layering diethyl ether onto a dichloromethane solution of the corresponding compound under a nitrogen atmosphere at room temperature. Data collection for **Fe2** and **Fe5** was carried out using mirror-monochromatic Cu-Kα radiation (λ = 1.54184 Å) at 170 K, cell parameters were obtained using global refinement of the positions of all collected reflections. Intensities were corrected for Lorentz and polarization effects and empirical absorption. The structures were solved by direct methods and refined with full-matrix least-squares on F^2. All hydrogen atoms were placed in the calculated positions. Structural solution and refinement were performed by using the Olex2 1.2 package and SHELXTL.[55] The SQUEEZE option of the crystallographic program PLATON was applied to remove free solvents from the structure of **Fe5**.[56] Details of the crystal data and processing parameters are summarized in Table S1 (ESI†).

Ethylene polymerization procedures

Ethylene polymerization at 1 atm ethylene pressure. The polymerization runs at 1 atm ethylene pressure were carried out in a Schlenk vessel. In a typical procedure, the iron precatalyst (2.0 μmol) was dissolved in toluene (30 mL) and the resulting solution stirred under an ethylene atmosphere (*ca.* 1 atm). The required amount of co-catalyst (MAO or MMAO) was then injected by syringe. The solution was then stirred at 60 °C (MAO) or 50 °C (MMAO) under 1 atm of ethylene pressure. After 30 min, the ethylene supply was disconnected and the vessel vented. The contents of the vessel were quenched with 10% hydrochloric acid in ethanol and the precipitated polyethylene collected by filtration. This was then washed with ethanol, dried under reduced pressure at 60 °C and then weighed.

Ethylene polymerization at 5 or 10 atm ethylene pressure. The polymerizations at 5 or 10 atm of ethylene pressure were carried out in a stainless steel autoclave (250 mL) equipped with mechanical stirrer, ethylene pressure control system and temperature controller. The autoclave was evacuated and then refilled with ethylene three times. Once the desired temperature was reached, the iron precatalyst (2.0 μmol) was dissolved in freshly distilled toluene (25 mL) in a Schlenk tube then injected into the autoclave, followed by the addition of another 25 mL of toluene. Subsequently, a specified amount of co-catalyst (MAO or MMAO) was injected and the final amount of toluene (50 mL) added by syringe. The autoclave was immediately pressurized with 5 or 10 atm pressure of ethylene and the stirring commenced. After the desired reaction time, the reactor was cooled with a water bath and the excess ethylene pressure released. The reaction solution was quenched and the polyethylene isolated as described for the 1 atm run.

Author contributions

Tian Liu: investigation, formal analysis, validation, writing – original draft. Yanping Ma: formal analysis, data curation, software. Gregory A. Solan: investigation, writing – review & editing. Yang Sun: investigation, validation. Wen-Hua Sun: conceptualization, funding acquisition, methodology, project administration, resources, supervision, writing – review & editing.

Conflicts of interest

There are no conflicts to declare.

Acknowledgements

References

1 B. L. Small, M. Brookhart and A. M. A. Bennett, *J. Am. Chem. Soc.*, 1998, **120**, 4049–4050.

2 G. J. P. Britovsek, V. C. Gibson, B. S. Kimberley, P. J. Maddox, S. J. McTavish, G. A. Solan, A. J. P. White and D. J. Williams, *Chem. Commun.*, 1998, 849–850.

3 G. J. P. Britovsek, M. Bruce, V. C. Gibson, B. S. Kimberley, P. J. Maddox, S. Mastroianni, S. J. McTavish, C. Redshaw, G. A. Solan, S. Strömberg, A. J. P. White and D. J. Williams, *J. Am. Chem. Soc.*, 1999, **121**, 8728–8740.

4 G. J. P. Britovsek, V. C. Gibson and D. F. Wass, *Angew. Chem., Int. Ed.*, 1999, **38**, 428–447.

5 G. J. P. Britovsek, V. C. Gibson, B. S. Kimberley, S. Mastroianni, C. Redshaw, G. A. Solan, A. J. P. White and D. J. Williams, *J. Chem. Soc., Dalton Trans.*, 2001, 1639–1644.

6 G. J. P. Britovsek, V. C. Gibson, S. K. Spitzmesser, K. P. Tellmann, A. J. P. White and D. J. Williams, *J. Chem. Soc., Dalton Trans.*, 2002, 1159–1171.

7 (*a*) V. C. Gibson, C. Redshaw and G. A. Solan, *Chem. Rev.*, 2007, **107**, 1745–1776; (*b*) V. C. Gibson and G. A. Solan, *Top. Organomet. Chem.*, 2009, **2**, 107–158; (*c*) V. C. Gibson and G. A. Solan, *Catalysis without Precious Metals*, ed. R. M. Bullock, Wiley-VCH, Weinheim, Germany, 2010, pp. 111–141.

8 Z. Wang, Q. Liu, G. A. Solan and W.-H. Sun, *Coord. Chem. Rev.*, 2017, **350**, 68–83.

9 S. Wang, D. Liu, R. Huang, Y. Zhang and B. Mao, *J. Mol. Catal. A: Chem.*, 2006, **245**, 122–131.

10 A. S. Abu-Surrah, K. Lappalainen, U. Piironen, P. Lehmus, T. Repo and M. Leskela, *J. Organomet. Chem.*, 2002, **648**, 55–61.

11 R. Gao, Y. Li, F. Wang, W.-H. Sun and M. Bochmann, *Eur. J. Inorg. Chem.*, 2009, 4149–4156.

12 K. Wang, K. Wedeking, W. Zuo, D. Zhang and W.-H. Sun, *J. Organomet. Chem.*, 2008, **693**, 1073–1080.

13 I. S. Paulino and U. Schuchardt, *J. Mol. Catal. A: Chem.*, 2004, **211**, 55–58.

14 M. J. Humphries, K. P. Tellmann, V. C. Gibson, A. J. P. White and D. J. Williams, *Organometallics*, 2005, **24**, 2039–2050.

15 W.-H. Sun, S. Jie, S. Zhang, W. Zhang, Y. Song and H. Ma, *Organometallics*, 2006, **25**, 666–677.

16 C. C. H. Atienza, C. Milsmann, E. Lobkovsky and P. J. Chirik, *Angew. Chem., Int. Ed.*, 2011, **50**, 8143–8147.

17 N. Kleigrewe, W. Steffen, T. Blömker, G. Kehr, R. Fröhlich, B. Wibbeling, G. Erker, J.-C. Wasilke, G. Wu and G. C. Bazan, *J. Am. Chem. Soc.*, 2005, **127**, 13955.

18 L. Xiao, R. Gao, M. Zhang, Y. Li, X. Cao and W.-H. Sun, *Organometallics*, 2009, **28**, 2225–2233.

19 S. Du, W. Zhang, E. Yue, F. Huang, T. Liang and W.-H. Sun, *Eur. J. Inorg. Chem.*, 2016, 1748–1755.

20 C. Bianchini, G. Giambastiani, I. R. Guerrero, A. Meli, E. Passaglia and T. Gragnoli, *Organometallics*, 2004, **23**, 6087–6089.

21 W. Zhang, W. Chai, W.-H. Sun, X. Hu, C. Redshaw and X. Hao, *Organometallics*, 2012, **31**, 5039–5048.

22 T. Liu, M. Liu, Y. Ma, G. A. Solan, T. Liang and W.-H. Sun, *Eur. J. Inorg. Chem.*, 2022, e20220396.

23 C. Görl and H. G. Alt, *J. Mol. Catal. A: Chem.*, 2007, **273**, 118–132.

24 S.-F. Yuan, L. Wang, Y. Yan, T. Liu, Z. Flisak, Y. Ma and W.-H. Sun, *RSC Adv.*, 2022, **12**, 15741–15750.

25 Q. Knijnenburg, S. Gambarotta and P. H. M. Budzelaar, *Dalton Trans.*, 2006, 5442–5448.

26 L. Zhang, W. Zhang, P. Serp, W.-H. Sun and J. Durand, *ChemCatChem*, 2014, **6**, 1310–1316.

27 M. W. Bouwkamp, E. Lobkovsky and P. J. Chirik, *J. Am. Chem. Soc.*, 2005, **127**, 9660.

28 S. Wang, B. Li, T. Liang, C. Redshaw, Y. Li and W.-H. Sun, *Dalton Trans.*, 2013, **42**, 9188–9197.

29 R. Raucoules, T. de Bruin, P. Raybaud and C. Adamo, *Organometallics*, 2009, **28**, 5358–5367.

30 Q. Mahmood, J. Guo, W. Zhang, Y. Ma, T. Liang and W.-H. Sun, *Organometallics*, 2018, **37**, 957–970.

31 A. S. Ionkin, W. J. Marshall, D. J. Adelman, B. B. Fones, B. M. Fish and M. F. Schiffhauer, *Organometallics*, 2006, **25**, 2978–2992.

32 W. Zhang, S. Wang, S. Du, C.-Y. Guo, X. Hao and W.-H. Sun, *Macromol. Chem. Phys.*, 2014, **215**, 1797–1809.

33 S. McTavish, G. J. P. Britovsek, T. M. Smit, V. C. Gibson, A. J. P. White and D. J. Williams, *J. Mol. Catal. A: Chem.*, 2007, **261**, 293–300.

34 L. Guo, H. Gao, L. Zhang, F. Zhu and Q. Wu, *Organometallics*, 2010, **29**, 2118–2125.

35 B. L. Small, R. Rios, E. R. Fernandez, D. L. Gerlach, J. A. Halfen and M. J. Carney, *Organometallics*, 2010, **29**, 6723–6731.

36 Q. Chen, W. Zhang, G. A. Solan, R. Zhang, L. Guo, X. Hao and W.-H. Sun, *Organometallics*, 2018, **37**, 4002–4014.

37 A. Boudier, P.-A. Breuil, L. Magna, H. Olivier-Bourbigou and P. Braunstein, *Chem. Commun.*, 2014, **50**, 1398–1407.

38 C. Huang, S. Du, G. A. Solan, Y. Sun and W.-H. Sun, *Dalton Trans.*, 2017, **46**, 6948–6957.

39 F. Huang, Z. Sun, S. Du, E. Yue, J. Ba, X. Hu, T. Liang, G. B. Galland and W.-H. Sun, *Dalton Trans.*, 2015, **44**, 14281–14292.

40 Z. Sun, F. Huang, M. Qu, E. Yue, I. V. Oleynik, I. I. Oleynik, Y. Zeng, T. Liang, K. Li, W. Zhang and W.-H. Sun, *RSC Adv.*, 2015, **5**, 77913–77921.

41 F. Huang, W. Zhang, E. Yue, T. Liang, X. Hu and W.-H. Sun, *Dalton Trans.*, 2016, **45**, 657–666.

42 Z. Zuo, Q. Zhang, M. Han, M. Liu, Y. Sun, Y. Ma and W.-H. Sun, *Catalysts*, 2022, **12**, 1119.

43 F. He, W. Zhao, X.-P. Cao, T. Liang, C. Redshaw and W.-H. Sun, *J. Organomet. Chem.*, 2012, **713**, 209–216.

44 J. Ramos, V. Cruz, A. Muñoz-Escalona and J. Martínez-Salazar, *Polymer*, 2002, **43**, 3635–3645.

45 N. E. Mitchell, W. C. Anderson Jr. and B. K. Long, *J. Polym. Sci. Part A: Polym. Chem.*, 2017, **55**, 3990–3995.

46 C. Huang, Y. Huang, Y. Ma, G. A. Solan, Y. Sun, X. Hu and W.-H. Sun, *Dalton Trans.*, 2018, **47**, 13487–13497.

47 H. Suo, I. I. Oleynik, C. Bariashir, I. V. Oleynik, Z. Wang, G. A. Solan, Y. Ma, T. Liang and W.-H. Sun, *Polymer*, 2018, **149**, 45–54.

48 Z. Wang, G. A. Solan, Q. Mahmood, Q. Liu, Y. Ma, X. Hao and W.-H. Sun, *Organometallics*, 2018, **37**, 380–389.

49 L. Guo, M. Zada, W. Zhang, A. Vignesh, D. Zhu, Y. Ma, T. Liang and W.-H. Sun, *Dalton Trans.*, 2019, **48**, 5604–5613.

50 W. Yang, Z. Ma, J. Yi and W.-H. Sun, *Catalysts*, 2017, **7**, 120.

51 M. Han, I. I. Oleynik, Y. Ma, I. V. Oleynik, G. A. Solan, X. Hao and W.-H. Sun, *Eur. J. Inorg. Chem.*, 2022, e202200224.

52 J. Yu, H. Liu, W. Zhang, X. Hao and W.-H. Sun, *Chem. Commun.*, 2011, **47**, 3257–3259.

53 W.-H. Sun, W. Zhao, J. Yu, W. Zhang, X. Hao and C. Redshaw, *Macromol. Chem. Phys.*, 2012, **231**, 1266–1273.

54 T. Liu, Y. Ma, G. A. Solan, T. Liang and W.-H. Sun, *Appl. Organomet. Chem.*, 2021, **35**, e6259.

55 G. M. Sheldrick, *Acta Crystallogr., Sect. A: Found. Adv.*, 2015, **A71**, 3–8.

56 G. M. Sheldrick, *Acta Crystallogr., Sect. C: Struct. Chem.*, 2015, **C71**, 3–8.

57 Q. Zhang, R. Zhang, M. Han, W. Yang, T. Liang and W.-H. Sun, *Dalton Trans.*, 2020, **49**, 7384–7396.

58 Q. Zhang, N. Wu, J. Xiang, G. A. Solan, H. Suo, Y. Ma, T. Liang and W.-H. Sun, *Dalton Trans.*, 2020, **49**, 9425–9437.

59 M. Zada, A. Vignesh, H. Suo, Y. Ma, H. Liu and W.-H. Sun, *Mol. Catal.*, 2020, **492**, 110981.

60 M. Han, Q. Zhang, I. I. Oleynik, H. Suo, G. A. Solan, I. V. Oleynik, Y. Ma, T. Liang and W.-H. Sun, *Dalton Trans.*, 2020, **49**, 4774–4784.

61 J. Guo, W. Zhang, I. I. Oleynik, G. A. Solan, I. V. Oleynik, T. Liang and W.-H. Sun, *Dalton Trans.*, 2020, **49**, 136–146.

62 L. Guo, W. Zhang, F. Cao, Y. Jiang, R. Zhang, Y. Ma, G. A. Solan, Y. Sun and W.-H. Sun, *Polym. Chem.*, 2021, **12**, 4214–4225.

63 M. Liu, S. Jiang, Y. Ma, G. A. Solan, Y. Sun and W.-H. Sun, *Organometallics*, 2022, **41**, 3237–3248.

64 A. W. Addison, T. N. Rao, J. Reedijk, J. Von Rijn and G. C. Verschoor, *J. Chem. Soc., Dalton Trans.*, 1984, 1349.